# Quantum conductance in double-wall carbon nanotubes grown by chemical vapor deposition

M. Baxendale
*Department of Physics, Queen Mary University of London, London E1 4NS, United Kingdom*

P. Battini and I. Pollini
*Dipartimento di Fisica, CNR-INFM, Università degli Studi di Milano, 20133 Milano, Italy*

M. Endo, Y. A. Kim, T. Hayashi, and H. Muramatsu
*Faculty of Engineering, Shinshu University, 4-17-1 Wakasato, Nagano-shi 380-8553, Japan*

(Received 10 June 2009; revised manuscript received 11 August 2009; published 16 September 2009)

The electronic conductance of networks of chemical vapor deposition grown double-wall carbon nanotubes comprising two populations of inner- and outer-wall diameter was measured by mechanically controllable break-junction methods. Two discrete conductances, $0.24G_0$ and $0.91G_0$ ($G_0=2e^2/h$), with nonideal corresponding transmission coefficients of 0.12 and 0.45, respectively, were identified as those of the lowest-energy metallic subbands in outer walls. High-bias injection was dominated by two discrete conductance values for a wide range of excitation energy.

DOI: 10.1103/PhysRevB.80.125411 PACS number(s): 72.80.Rj, 73.23.Ad, 73.63.Fg

## I. INTRODUCTION

Carbon nanotubes have attracted interest due to their potential nanoscale electronic-device applications. They are graphitic cylinders of nanometer-scale diameter and micrometer-scale length; this topology, combined with the absence of defects on a mesoscopic scale, gives rise to uncommon electronic properties of individual single-wall nanotubes (SWNT), which, depending on their diameter and chirality, can be metallic or semiconducting.[1,2] The landmark paper of Frank *et al.*[3] provided evidence for ballistic conduction in pristine freely suspended multiwall carbon nanotubes (MWNT). Subsequent research has confirmed ballistic transport in MWNT bundles at room temperature[4–8] and that the ballistic conduction in nanotubes is the result of a high degree of structural integrity and a low level of inelastic scattering. The ballistic conductance regime is governed by the Landauer-Büttiker equation[9]

$$G = G_0 \Sigma_{\alpha\beta} T_{\alpha\beta}, \tag{1}$$

where $G_0=2e^2/h$ ($G_0^{-1}=12900\ \Omega$) is the conductance quantum and $T_{\alpha\beta}$ is the transmission probability of an electron going from channel $\alpha$ to channel $\beta$, with $\alpha$ and $\beta$ representing the excited bands involved in the transport.[10,11] The conductance of series one-dimensional (1D) ballistic wires with an arbitrary number of contacts and scattering centers is given by

$$G = G_0\left[\sum (g_j)^{-1}\right]^{-1}, \tag{2}$$

where the summation is over the number of wires in series and $g_j$ is the conductance of wire $j$.[12]

Theory predicts two conductance channels for an individual metallic SWNT with ideal contacts and unity transmission coefficient, resulting in a conductance $G=2G_0^3$. However, the theoretical value of $2G_0$ for SWNTs may not be observed in each shell of a MWNT, resulting in conductance values lower than $2G_0$ in an experiment; the interwall interaction is likely to reduce the conductance values below $2G_0$, as described by Sanvito *et al.*[13] The double-wall carbon nanotube (DWNT) is the archetypal system for elucidating the role of interwall interactions in MWNTs.

This investigation is devoted to quantum conductance studies of networks comprising individual chemical vapor deposition (CVD)-grown DWNTs of well-defined inner and outer diameter. The aim is to elucidate interwall interaction effects on the transport properties in DWNTs. The dispersion in diameter and interwall separations for this CVD-grown DWNT sample is superior to that of DWNTs produced by the $C_{60}$-SWNT coalescence method[14] used in our previous study[8] and is therefore closer to the ideal of a completely phase-pure DWNT sample.

The mechanically controllable break-junction (MCBJ) methods used have the advantage of easing the sample preparation using milligram quantities of material and conductance sampling for a statistically large number of nanotubes.[8] No chemical modification, other than exposure to the atmosphere, or exposure to harsh chemical environments is required for sample preparation hence there is a high degree of confidence that the measurement probes the intrinsic electronic structure.

Some electrical measurements on MWNT (Refs. 6 and 7) show that the conductance can be quantized in units of $1G_0$; by immersing MWNT at the tip of a bundle into liquid metal mercury with an almost ideal contact, Frank *et al.*[3] observed odd multiples of $G_0$ and noninteger conductance values, such as $G=0.5G_0$. A complete description of the quantized transport requires consideration of the interwall interaction, as in the case of graphite, however other phenomena have been evoked in the literature.[15,16] Other experiments on SWNTs and MWNTs have demonstrated ballistic transport with conductance steps at even multiples of $G_0$,[6,7] and the realization of negligibly small contact resistances. The results reported by Kong *et al.*[5] and Urbina *et al.*[6] have shown that two channels for electron transport exist in a metallic SWNT, as predicted theoretically. Many explanations have been given for the one open channel in SWNTs and the $G=1G_0$ values in MWNTs, invoking interwall interactions,[3] an opaque $\pi$

 

channel,[16] and antiresonance with edge states in inner tubes.[17] In particular, Choi *et al.*[16] have given an explanation for the $1G_0$ conductance value in metallic SWNT by means of a model based on an *ab initio* nonlocal pseudopotential conductance calculation for nanotubes with one end immersed in a jellium metal. In nonideally contacted nanotubes the transmission coefficients may be less than unity (the conductance less than $2G_0$) due to backscattering and imperfect contacts. Point defects and surface contaminants can also depress the conductance by $\Delta G_0=1$ for a 1.4-nm-diameter SWNTs.[18] The work of Poncharal *et al.*[4] reported values of $0.6G_0$ and $0.8G_0$ as the most frequently observed noninteger values of the conductance from protruding bundles. Recently, we have observed similar results in pristine, freestanding SWNT and DWNT systems at room temperature,[8] and concluded that SWNTs are two-channel ballistic conductors with a transmission coefficient of 0.88. We have also suggested these DWNTs, produced by the coalescence method, are approximately one-channel ballistic conductors with additional field- and temperature-dependent two-channel contributions.[8] Interpretation of the coalescence-produced DWNT conductance data was limited by the large dispersion in inner- and outer-wall diameter and interlayer separation.

## II. EXPERIMENT

Two characteristics of DWNT structure are known: the lattice structure of inner and outer walls are not correlated, i.e., the lattice of the outer tube is incommensurate with that of the inner (although some commensurate tubes are also known); and that the difference between the radius of the inner and outer tubes is about 3.6 Å, independent of the circumference of the DWNT.[19] Raman spectroscopic radial breathing mode (RBM) analysis and direct TEM imaging of the DWNTs used in this study revealed four diameters: 0.77, 0.90, 1.43, and 1.60 nm, that correspond to DWNT structures with inner-to-outer diameter ratios 0.77:1.43 and 0.90:1.60.[20] The difference between the radius of the inner and outer walls of the DWNTs is: $\Delta R_1=(1.43-0.77)/2=0.33$ nm $=3.3$ Å and $\Delta R_2=(1.60-0.90)/2=0.35$ nm$=3.5$ Å, respectively, in agreement with the results of Bandow *et al.*[19] Details of the DWNT synthesis and characterization can be found in Ref. 20.

The peak position of van Hove singularities ($E_{vHS}$) in the 1D density of states for all nanotube diameters, $d_t$, in the range 6–18 Å relative to the Fermi energy ($E_F$) from the tight-binding calculation of Saito *et al.*[21] are plotted in Fig. 1. Van Hove singularities occur at the energy corresponding with the bottom of a subband. In this figure the 0.77, 0.90, 1.43, and 1.60 nm diameters extracted from RBM analysis are plotted as shaded ranges of diameter that correspond to an error in the observed RBM frequency, that is, typical for a Raman spectrometer, namely, $\pm 4$ cm$^{-1}$; the DWNT diameter pairings of 0.77:1. Possibilities for combining semiconducting and metallic nanotubes to compose the DWNT structures used in 43 and 0.90:1.60 are differentially shaded. Clearly the ranges of diameter for the inner and outer DWNT walls span both metallic and semiconducting band structures therefore there are four this study.

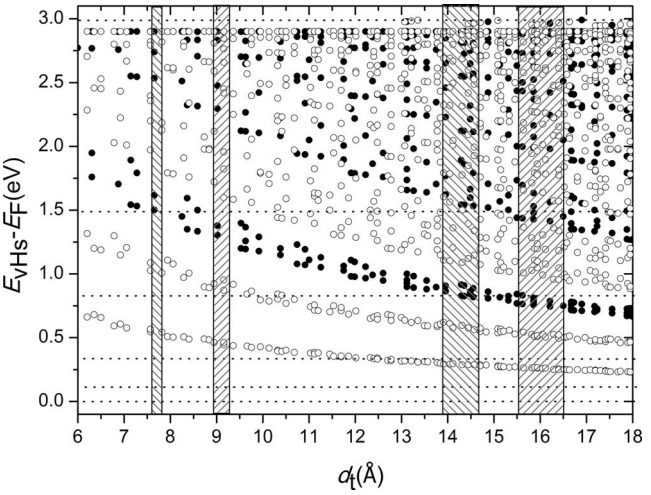


FIG. 1. $E_{vHs}$-$E_F$ versus nanotube diameter for $d_t=6-18$ Å (from the tight-binding calculation in Ref. 21.) Open circles refer to semiconducting subbands and closed circles to metallic subbands. Dotted horizontal lines refer to injection energies corresponding to the bias voltages used in this study: $V=2$ mV, $V=0.1$ V, $V=0.3$ V, $V=0.8$ V, $V=1.5$ V, and $V=3.0$ V. Shaded ranges of $d_t$ are centered on the four diameters extracted from RBM analysis of the DWNT sample; the limits are fixed by the assumption of $\pm 4$ cm$^{-1}$ in the Raman signal.

The MCBJ methods used in this study are detailed in Ref. 8: an 8-bit method centered on a electromechanical relay and a 16-bit method based on a conventional scanning tunneling microscope (STM). The higher-resolution STM-based MCBJ was in the low-bias regime and the relay-based MCBJ method for high-bias measurements; in both cases conductance histograms were composed from the accumulated data of 30 measurement cycles (i.e., $3\times 10^4$ data points). The STM-based MCBJ method offers the possibility of a limited range of elevated temperature and the use of several counter-electrode materials, such as thin-film Au, liquid Hg, and highly oriented pyrolitic graphite (HOPG).

## III. RESULTS AND DISCUSSION

A conductance histogram (bin size$=0.01G_0$) obtained from the STM-based MCBJ method with a HOPG counter electrode and bias across the DWNT network of $V=0.2$ mV is given in Fig. 2. The $<1G_0$ conductance peaks observed in data obtained from measurements performed under the conditions described above using the three electrode materials used in this study are highlighted in Fig. 2. The significance of this $<1G_0$ range of peaks is that the values can give an indication of the intrinsic number of channels supported by an individual wire if the $<1G_0$ peaks are due to series combinations via Eq. (2). Clearly values of conductance expected from low-membered series combinations of one-channel wires $(0.50G_0, 0.33G_0, 0.25G_0, \ldots)$ or two-channel wires $(0.66G_0, 0.50G_0, 0.40G_0, \ldots)$ could account for most of the fractional conductance values commonly observed in this system. However, the $0.74G_0$, $0.84G_0$, and $0.92G_0$ values cannot be readily explained in terms of a low-

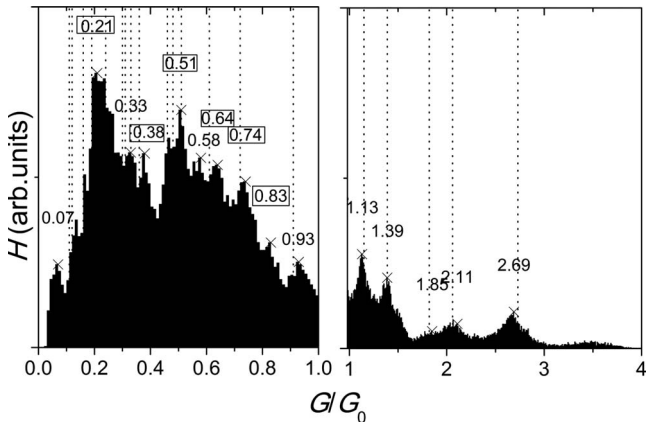


FIG. 2. Conductance histogram for the DWNT sample obtained from the STM-based MCBJ method with a HOPG counter electrode (bin size=$0.01G_0$). The frequency of conductance value $G_i$ is defined by $H(G_i)=N_i/N\Delta G_i$, where $N_i$ is the data points in voltage-bin number $i$ accumulated from all closed-open cycles, $N$ is the total number of data points, and $\Delta G_i$ is the conductance bin size. Highlighted $<1G_0$ peaks are common the conductance data from several counter-electrode materials: thin-film Au, liquid Hg, and HOPG. Vertical dotted lines represent the conductance values with greater than 1% probability of formation through series and parallel combinations of the discrete conductances $0.24G_0$ and $0.91G_0$ calculated using the model described in the text.

membered series model of integer-channel wires. A simple interpretation of the complete range of conductance peaks requires a correspondence between those conductance values due to parallel combinations of quantum resistors and those values that arise from series connections of the same quantum resistance values via Eqs. (1) and (2). The challenge is to account for the range of observed conductance peaks in Fig. 2 in terms a simple model, in particular, the fractional $<1G_0$ conductance values common to all measurements independent of counter-electrode material.

Numerical modeling was used to calculate the most probable network configurations of quantum resistors in series and parallel combinations by calculation of the conductance of: (i) $n$-membered series connections of individual wire conductance $g$, where $n$ is a positive integer randomly generated with a normally distributed probability (centroid=1, standard deviation=1); and (ii) $p$-membered parallel connections of individual wire conductance $g$, where $p$ is a positive integer randomly generated with a normally distributed probability (centroid=1, standard deviation=1), via Eqs. (1) and (2). Peaks in the histograms of frequency versus conductance with $0.01G_0$ bin size were identified for those values with greater than 1% probability of formation by assuming an equal probability of a series or parallel combination spanning the electrodes for $10^4$ closed-open measurement cycles.

The distribution of conductance peaks in Fig. 2 was investigated with reference to the model. The distribution of the $>1G_0$ features clearly points to noninteger values of individual wire conductance. The $0.93G_0$, $1.85G_0$, $2.69G_0$ series of peaks suggests a 1–3 parallel wires of conductance $0.93G_0$. There is evidence for the two-membered series combinations of the $0.93G_0$ at $0.46G_0$ (although this is feature was not resolved). The distribution of peaks $>0.93G_0$ also suggests the possibility of a parallel combination with $\sim 0.2G_0$ wire (e.g., $1.13G_0=0.93G_0+0.2G_0$); the presence of such a wire is supported by the strong feature at $\sim 0.2G_0$. The possibility of two discrete conductances in the network was therefore introduced to the model by allowing equal probability of either being selected. Optimal agreement of experimental data with the values determined by the model was achieved for the two discrete conductances $0.24G_0$ and $0.91G_0$; the values generated by the model are marked by dotted vertical lines in Fig. 2. There is high degree if confidence in this result since it accounts for the $>1G_0$ features, has good agreement with five of the six conductance peaks that are common to all measurements (the feature at $0.83G_0$ can has a greater than 1% creation probability when the standard deviation in the distribution of parallel connections is increased from one to three), and clustering of expected peaks at $\sim 0.2G_0$, $\sim 0.3G_0$, $\sim 0.5G_0$, and absence of features at $\sim 0.4G_0$ corresponds with maxima and minima in the experimental data. No other choices of either a single-channel number or two-channel numbers have given this quality of agreement. Furthermore agreement with $>1G_0$ features is very sensitive to the choice(s) of discrete conductance.

The values of the two discrete conductances extracted from the analyses described for the complete range of bias used in this study referred to above and below are given in Table I. The interpretation of the discrete conductance values in Table I was made with reference to Fig. 1. In the STM-based MCBJ method the bias is constant throughout the closed-open MCBJ cycle, whereas the circuit configuration used in the electromechanical relay-based MCBJ is such that $V$ increases with time during a closed-open MCBJ cycle. Conductance data obtained using electromechanical relay-based MCBJ method can be therefore viewed as comprising contributions from subbands of energy lower than the maximum injection energy eV.

The electromechanical relay-based MCBJ was used to investigate the bias dependence of the conductance. The conductance histogram obtained for $V=0.1$ V is given in Fig. 3(a). In agreement with our previous report concerned with DWNTs produced by the coalescence method, the increase in bias level is accompanied by the appearance of a broad feature centered at $\sim 3G_0$.[8] Careful analysis of the distribution of conductance peaks, using the modeling method described above, revealed optimum correspondence with that distribu-

TABLE I. Discrete conductance values extracted from the data in Figs. 2–4 using the analyses described in the text.

| $V$ (V) | 0.0002 | 0.1 | 0.3 | 0.8 | 1.5 | 3.0 |
|---|---|---|---|---|---|---|
| $G/G_0$ | 0.24 | 0.91 | 1.50 | 3.76 | 4.75 | 5.01 |
| | 0.91 | 3.00 | 3.60 | 5.30 | 7.34 | 7.94 |

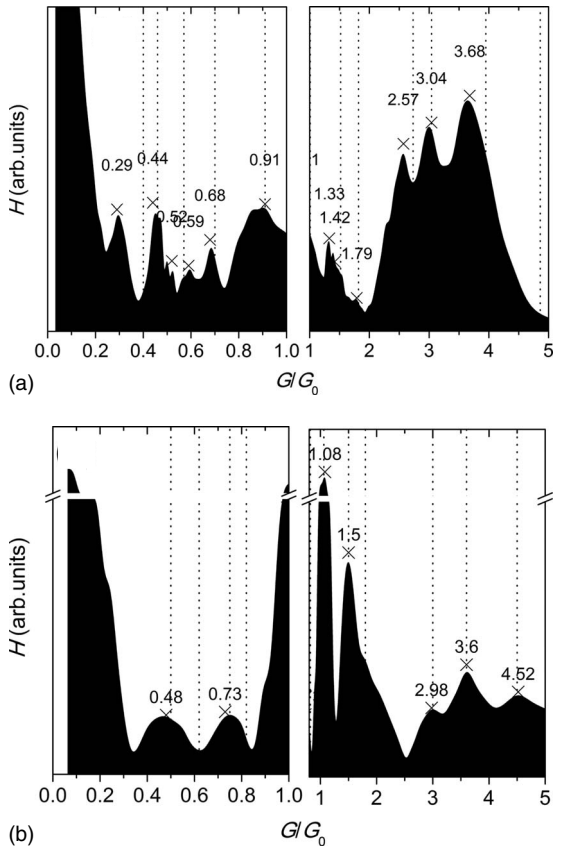


FIG. 3. Conductance histograms obtained using the electromechanical relay MCBJ method for: (a) $V=0.1$ V and (b) $V=0.3$ V. Vertical dotted lines represent the conductance values with greater than 1% probability of formation through series and parallel combinations of the discrete conductances: (a) $0.91G_0$ and $3.00G_0$, (b) $3.60G_0$ and $1.5G_0$, calculated using the model described in the text.

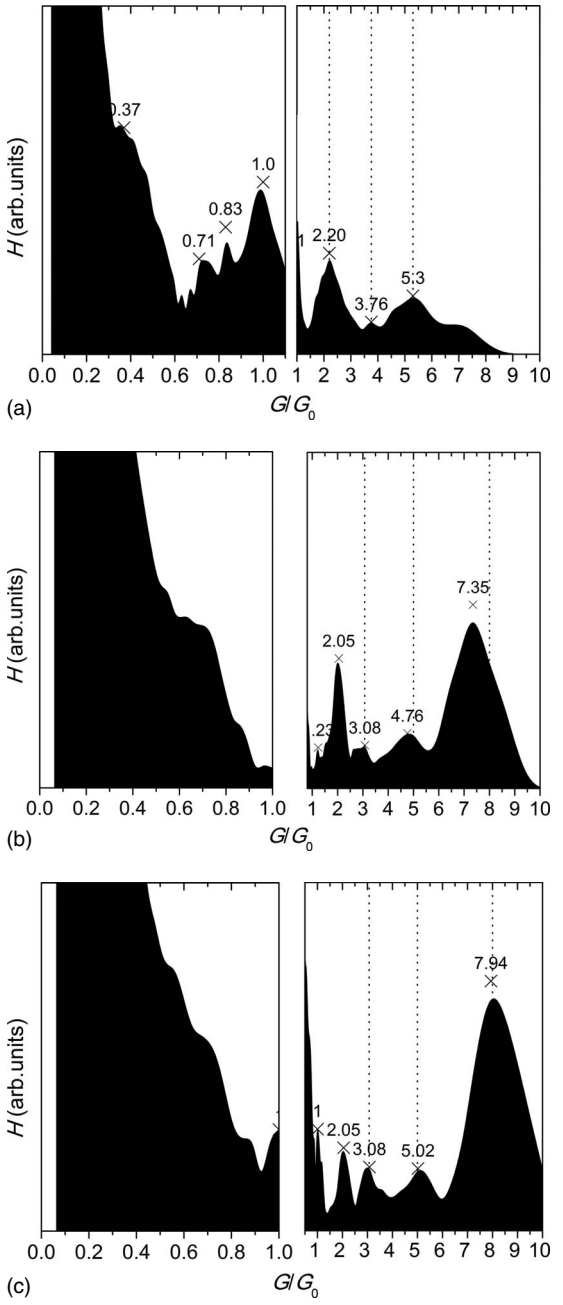


FIG. 4. Conductance histograms obtained using the electromechanical relay MCBJ method for: (a) $V=0.8$ V, (b) $V=1.5$ V, and (c) $V=3.0$ V. Vertical dotted lines represent the two discrete conductance values (the higher two values) and series combination of these discrete values (the lower value).

tion due to series and parallel combinations two discrete conductances $0.91G_0$ and $3.0G_0$; the values generated by the model are marked by dotted vertical lines in Fig. 3(a). Similarly; in Fig. 3(b) the discrete conductances extracted in the same way for $V=0.3$ V are $3.60G_0$ and $1.50G_0$.

The range of metallic and semiconducting subbands embraced by the inner- and outer-wall diameters present in the sample is such that there is a possibility of both conductivity types in both walls of both DWNT diameter pairings. The lowest-energy semiconducting subbands occur in the outer and inner walls at $E_{vHs}$-$E_F$ energy ~0.3 and ~0.5 eV, respectively. Conductance data gleaned from the $V=0.2$ mV and $V=0.1$ V bias values therefore can be attributed to metallic conduction in states close to $E_F$ in metallic outer walls. Ideal metallic inner and outer DWNT walls are expected to each contribute two conductance quantum units giving a total conductance of $4G_0$ per DWNT.[16] If the two discrete conductance values observed at mV bias are due to contributions from the two populations of DWNT diameter pairings in the sample, then clearly metallic conduction is nonideal; assuming the $0.91G_0$ and $0.24G_0$ discrete conductance values are due to outer-wall conduction, these correspond to transmission coefficients of 0.45 and 0.12, respectively. The emergence of $3G_0$ discrete conductance value at $V=0.1$ V is unlikely to be the result of significant injection into the first semiconducting subband at ~0.3 eV of the outer wall of a semiconducting outer-wall/metallic inner-wall DWNT given the difference in injection energy and $E_{vHs}$. The most likely explanation for this feature is bias-dependent injection with contributions of $\sim 1G_0$ from a metallic outer wall and $2G_0$ from a metallic inner wall as we previously postulated for coalescence-produced DWNT networks.[8]

In the absence of bias-dependent injection we would expect the $V=0.2$ mV (Fig. 2) and $V=0.1$ V [Fig. 3(a)] conductance histograms extracted from the two MCBJ methods

to be identical. The $0.91G_0$ discrete conductance is common to both while the other identified discrete conductance values shifts from $0.24G_0$ to $3.0G_0$ in this bias range. It is difficult to state whether a signal from a $0.24G_0$ subband remains in the $V=0.1$ V conductance histogram since $<0.25G_0$ features are not fully resolved.

The $\sim 1G_0$ conductance is ubiquitously observed in large diameter MWNT systems in which the outer walls are effectively metallic; we therefore conclude this value is due to the metallic outer-wall population of DWNTs. Possible explanations for the this result were first pointed out by Frank *et al.* and subsequently by many other authors.[15,16] Two different interpretations try to link the "missing" conductance quantum either to the interface resistance and contact defects in the system or to the splitting of the double degenerate metallic level. In the first case, we should expect the transmission coefficient to be a random variable varying in the range 0.3–0.7[4]. However, as we have found a value $G \sim 1G_0$ in all histograms at room temperature and for small electrical excitation, and not a range of $G$ values, we propose that this result is due to lifting of the degeneracy in the metallic band.

The conductance histograms for $V=0.8$, 1.5, and 3 V are characterized by the emergence of a conduction peak at $2G_0$ and three broad $>2G_0$ peaks comprising two discrete conductances (the upper two values) and series combination of the discrete values (the lower value); the two discrete conductances and the series combination are marked by dotted vertical lines in Fig. 4. We attribute the higher discrete conductances and $2G_0$ features that emerge for $V>3$ V as being due to the enhanced probability of semiconducting outer-wall/semiconducting inner-wall and metallic outer-wall/semiconducting inner-wall DWNTs and excitation into higher level metallic and semiconducting subbands contributing to the network conduction for $E_{\mathrm{vHs}}$-$E_{\mathrm{F}}>3$ eV, Fig. 1. Exact mapping of the high-bias conductance data onto the current-carrying subband distribution will require a single-phase DWNT population.

## ACKNOWLEDGMENTS

This work was partially supported by the CLUSTER project (second stage) and a grant for Specially Promoted Research (Grant No. 19002007) from the Ministry of Education, Culture, Sports, Science and Technology of Japan.

[1] R. Saito, G. Dresselhaus, and M. S. Dresselhaus, *Physical Properties of Carbon Nanotubes* (Imperial College, London, 1998).
[2] J. W. Mintmire, B. I. Dunlap, and C. T. White, Phys. Rev. Lett. **68**, 631 (1992).
[3] S. Frank, P. Poncharal, Z. L. Wang, and W. A. De Heer, Science **280**, 1744 (1998).
[4] P. Poncharal, C. Berger, Y. Yi, Z. L. Wang, and W. A. de Heer, J. Phys. Chem. B **106**, 12104 (2002).
[5] J. Kong, E. Yenilmez, T. W. Tombler, W. Kim, H. Dai, R. B. Laughlin, L. Liu, C. S. Jayanthi, and S. Y. Wu, Phys. Rev. Lett. **87**, 106801 (2001).
[6] A. Urbina, I. Echeverría, A. Pérez-Garrido, A. Díaz-Sánchez, and J. Abellán, Phys. Rev. Lett. **90**, 106603 (2003).
[7] M. Kociak, K. Suenaga, K. Hirahara, Y. Saito, T. Nakahira, and S. Iijima, Phys. Rev. Lett. **89**, 155501 (2002).
[8] M. Baxendale, M. Melli, Z. Alemipour, I. Pollini, and T. J. S. Dennis, J. Appl. Phys. **102**, 103721 (2007).
[9] M. Büttiker, IBM J. Res. Dev. **32**, 63 (1988).
[10] R. Landauer, IBM J. Res. Dev. **1**, 223 (1957).
[11] R. Landauer, Philos. Mag. **21**, 863 (1970).
[12] W. A. de Heer, S. Frank, and D. Ugarte, Z. Phys. B: Condens. Matter **104**, 469 (1997).
[13] S. Sanvito, Y. K. Kwon, D. Tománek, and C. J. Lambert, Phys. Rev. Lett. **84**, 1974 (2000).
[14] A. Hashimoto, K. Suenaga, K. Urita, T. Shimada, T. Sugai, S. Bandow, H. Shinohara, and S. Iijima, Phys. Rev. Lett. **94**, 045504 (2005).
[15] H. J. Li, W. G. Lu, J. J. Li, X. D. Bai, and C. Z. Gu, Phys. Rev. Lett. **95**, 086601 (2005).
[16] H. J. Choi, J. Ihm, Y. G. Yoon, and S. G. Louie, Phys. Rev. B **60**, R14009 (1999).
[17] S. Uryu, Phys. Rev. B **69**, 075402 (2004).
[18] L. Chico, L. X. Benedict, S. G. Louie, and M. L. Cohen, Phys. Rev. B **54**, 2600 (1996).
[19] S. Bandow, M. Takizawa, K. Hirahara, M. Yudasaka, and S. Iijima, Chem. Phys. Lett. **337**, 48 (2001).
[20] M. Endo, H. Muramatsu, T. Hayashi, Y. A. Kim, M. Terrones, and M. S. Dresselhaus, Nature (London) **433**, 476 (2005).
[21] R. Saito, G. Dresselhaus, and M. S. Dresselhaus, Phys. Rev. B **61**, 2981 (2000).